Desalination and Water Treatment
www.deswater.com

doi: 10.5004/dwt.2018.22858

127 (2018) 132–139
September

Use of halloysite–TiO_2 nanocomposites for the decomposition of tebuconazole fungicide in water

D. Panagiotaras[a,*], V. Bekiari[b], E. Stathatos[c], D. Papoulis[d], G. Panagopoulos[a], A.N. Kalarakis[a], I. Iliopoulos[a], E. Kourkouta[a], P. Mavrokota[a]

[a]*Department of Mechanical Engineering Technological Educational Institute of Western Greece, 263 34 Patras, Greece, emails: sakpanag@teiwest.gr (D. Panagiotaras), gpanagopoulos@teiwest.gr (G. Panagopoulos), a_kalarakis@teiwest.gr (A.N. Kalarakis), johniliop1995@yahoo.gr (I. Iliopoulos), eirinixiomi@hotmail.com (E. Kourkouta), panmavrokota@gmail.com (P. Mavrokota)*
[b]*Department of Fisheries & Aquaculture Technology, Technological Educational Institute of Western Greece, Messolonghi, Nea Ktiria, 30200 Messolonghi, Greece, email: mpekiari@teimes.gr*
[c]*Nanotechnology and Advanced Materials Laboratory, Department of Electrical Engineering, Technological Educational Institute of Western Greece, 263 34 Patras, Greece, email: estathatos@teiwest.gr*
[d]*Department of Geology, University of Patras, 265 04 Patras, Greece, email: papoulis@upatras.gr*

Received 13 February 2018; Accepted 25 July 2018

ABSTRACT

In this study we present halloysite clay mineral combined with TiO_2, as promising new class of nanomaterials that can be used as an effective, cost-efficient, and environment-friendly procedure for the decomposition of tebuconazole, $C_{16}H_{22}ClN_3O$, [(RS)-1-*p*-chlorophenyl-4,4-dimethyl-3-(1H-1,2,4-triazol-1-ylmethyl)-pentan-3-ol], TEB-fungicide, in water. For this purpose, halloysite–TiO_2 nanoparticles are prepared using the sol-gel methodology combined with hydrothermal treatment of the samples in mild conditions. The halloysite–TiO_2 nanocomposites are characterized by X-ray diffraction, scanning electron microscopy, transmission electron microscopy, and N_2 sorption–desorption isotherms analysis by Brunauer–Emmett–Teller to determine specific surface area (SSA). The total pore volume of the halloysite 40%–TiO_2 60% prepared nanocomposite and its SSA are 0.35 cm^3/g and 188 m^2/g, respectively. This nanocomposite showed a photocatalytic efficiency of 39.5% to TEB decomposition after 240 min under UV irradiation. The halloysite 30%–TiO_2 70% nanocomposite has a total pore volume of 0.34 cm^3/g and a SSA of 187 m^2/g. This nanomaterial shows 40.0% photocatalytic efficiency for TEB destruction under UV exposure. The best photodegradation efficiency, 47.4% of TEB was achieved with the halloysite 10%–TiO_2 90% nanomaterial, instead of 33.2% decomposition efficiency measured when commercial TiO_2 (Degussa P25) was used. In this case, the halloysite 10%–TiO_2 90% nanocomposite showed the highest SSA of 222 m^2/g. The concentration of TEB did not show any significant change in all the samples after 150 min exposure under UV illumination.

Keywords: Fungicide; Photocatalysis; Tebuconazole; Halloysite; TiO_2 nanocomposites

1. Introduction

The remarkable and rapid socio-economic development over the past few decades has further stressed the hydrogeological system. In many areas, locally and worldwide, population affected by diseases related with the consumption of unsuitable water, containing mainly bacteriological, organic, and inorganic pollutants [1,2]. Fresh and ground water contamination by pesticides is a subject of a great importance affecting a big number of people living mainly in areas with intense agricultural activities [3,4]. The effects of

* Corresponding author.

Presented at the 15th International Conference on Environmental Science and Technology (CEST-2017), 31 August–2 September 2017, Rhodes, Greece.

past and present land-use practices become apparent in fresh and ground water contamination and there is an increasing need for the development of water purification technologies. Among them, advanced oxidation processes (AOPs) have been used as effective methods for the photocatalytic degradation of pesticides in the natural environment [5]. The application of AOPs for the mineralization of persistent organic pollutants like pesticides, in aqueous solutions is very effective because of the generation of hydroxyl radicals (•OH) and other oxidative chemical species, which have a very strong destruction effect. Among other techniques, such as Fenton's reagent, ozone, UV/ozone, and UV/H_2O_2, the use of heterogeneous photocatalysis using semiconductor TiO_2 as a catalyst for the oxidation of pesticides and other pollutants have been extensively studied [5–10].

The high efficiency of TiO_2 to produce hydroxyl radicals in solution under UV light illumination, the high stability in water and the nontoxic response are major characteristics. In addition, TiO_2 is a cost-efficient and very effective photocatalyst for the decomposition of organic substances in water and air [11–13]. The •OH compounds are very reactive chemicals with a redox potential of +2.8 V (vs NHE) and they can react with the organic pollutants with a 10^7–10^{10} M^{-1} s^{-1} constant reaction rate [14,15]. The end product of the reaction of the •OH radicals with the organic compounds are CO_2, H_2O, and inorganic salts [14–17]. Because of hydroxyl radicals' high redox potential (+2.8 V), they are more effective for the decomposition of organic pollutants than other oxidants like O_3 (+2.07 V), HOCl (+1.49 V), and H_2O_2 (+1.78 V) used for water purification and disinfection [14–17]. In addition, the effectiveness of semiconductors for photoactivation is a function of the energy required for the excitation of their crystals. For TiO_2 in the anatase form this energy must be higher than the band gap energy of E_g = 3.2 eV and for the rutile higher than E_g = 3.0 eV. As a conclusion TiO_2 nanocrystals excitation requires energy in the near UV region (radiation with $\lambda \leq 380$ nm for anatase and $\lambda \leq 400$ nm for rutile) [18].

The TiO_2/UV technique is based on the UV irradiation of the TiO_2 and the generation of electron (–)/(+) holes pairs which in aqueous system produce the reactive redox chemical species onto the catalyst surface [19]:

$$TiO_2 + h\nu \rightarrow e^-_{cb} + h^+_{vb} \quad (1)$$

$$O_2 + e^-_{cb} \rightarrow O_2^{-\bullet} \quad (2)$$

$$H_2O + h^+_{vb} \rightarrow {}^\bullet OH + H^+ \quad (3)$$

The main oxidizing agents produced are •OH and $O_2^{-\bullet}$ radicals which react with the organic pollutants, e.g., pesticides to produce intermediates and CO_2 and H_2O as the end products.

This paper examines the decomposition rate of tebuconazole (TEB) which is a common fungicide used in agricultural applications all over Europe. It belongs to the triazoles group of toxic-organic substances, in concentrations up to 18.72 μg/L in natural waters [20]. TEB is a biorefractory contaminant which cannot be degraded using conventional techniques and limited studies are available for the photocatalytic treatment of this fungicide. The most common photocatalyst used for the degradation of TEB in water suspensions is TiO_2 [20–22]. However, new studies show that new materials as clay minerals and others combined with TiO_2 can be used as efficient photocatalysts for water purification purposes [23–28].

To this perspective we synthesized clay mineral-based nanocomposites, halloysite–TiO_2 and used them for the degradation of TEB fungicide in aqueous solution. The characterization and photocatalytic efficiency of the new class of material is presented.

2. Methodology

2.1. Materials and chemical reagents

A halloysite sample from Utah, USA was used for the synthesis of the Hal-TiO_2 nanocomposites. Titanium tetraisopropoxide, $Ti(OC_3H_7)_4$, HCl acid, nanopure water (triple distilled-3D), and absolute ethanol were used for the preparation of the TiO_2 sol dispersion. Tebuconazole, $C_{16}H_{22}ClN_3O$, [(RS)-1-*p*-chlorophenyl-4,4-dimethyl-3-(1H-1,2,4-triazol-1-ylmethyl)-pentan-3-ol], was used for the fungicide samples preparation. Commercial TiO_2 (P25-TiO_2) used as standard photocatalyst has an anatase to rutile ratio 80:20, average particle size 20 nm, and particle specific area ~50 m^2/g. All reagents were of analytical grade commercially available from Merck (KGaA) and Sigma-Aldrich (Germany). A stock TiO_2 sol dispersion was prepared by mixing titanium tetraisopropoxide, $Ti(OC_3H_7)_4$, with hydrochloric acid, nanopure water (3D), and absolute ethanol. The TiO_2 stock dispersion was diluted in absolute ethanol, stirred for 2 h and then a halloysite–water dispersion was added. The slurry was stirred for 24 h and the resulting dispersion was washed with 3D water and centrifuged. The halloysite–TiO_2 composites were treated in mild hydrothermal conditions in an autoclave for 5 h at 180°C. The detailed methodology was used for the preparation of the halloysite–TiO_2 nanocomposites is described by Papoulis et al. [24]. In order to study the photocatalytic performance of the halloysite–TiO_2 materials, we examined five samples with three different weight ratios of TiO_2 over halloysite, namely TiO_2/halloysite = 3/2, 7/3, and 9/1, pristine TiO_2 (P25-TiO_2) and halloysite as the rest two samples. In addition, we have chosen the TEB concentration as 1 mg/L. The mass/volume ratio was 0.1375 g of catalyst/250 mL of TEB solution, in order to give 550 mg/L of catalyst concentration in the solution [20].

2.2. Instrumentation

X-ray diffraction (XRD) patterns for the determination of the phase compositions of TiO_2 treated halloysite samples were monitored with Bruker D8 advance diffractometer, with Ni-filtered CuKα radiation. Halloysite–TiO_2 morphology was examined by field emission scanning electron microscopy (FE-SEM), FEI inspect TM F50. In order to investigate TiO_2 dispersion on clay mineral surfaces a transmission electron microscopy (JEOL JEM-2100 electron microscope) operating at an acceleration voltage of 200 kV was also used. Nitrogen sorption–desorption isotherms for each sample degassed at 100°C for 3 h were obtained with a Micromeritics Tristar 3000 and the surface area, porosity, and pore size distribution were derived by differentiating them according to Brunauer–Emmett–Teller (BET) method. For the photocatalytic tests, a cylindrical reactor was used in all experiments (Fig. 1). Four

Fig. 1. Photographs showing the samples preparation and photocatalytic reactor used in all experiments.

black light fluorescent tubes of 4 W each nominal power were placed around the reactor. The whole construction was covered with a cylindrical aluminum reflector. Before the UV illumination, we applied continuous stirring to the samples, for 15 min in the dark in order to achieve the zero point of adsorption prior to the photocatalytic tests. Cooling was achieved by air flow from below the reactor using a ventilator. Continuous stirring of the samples in the reactor was achieved with a magnetic stirrer.

The intensity of radiation was measured with a Solar Light PMA-2100 UV-Photometer and found equal with 0.9 mW/cm^2. The reactor was filled with 200 mL of the sample and the irradiation applied for a total of 300 min. Total organic carbon (TOC) analysis was performed using the combustion-infrared method, Standard Method (SM) 5310B (Standard Methods for the Examination of Water and Waste Water, American Water Works Association) [29,30]. All analyses were carried out using a Shimadzu TOC analyzer (TOC-VCSH).

3. Results and discussion

Three different ratios of TiO_2 nanoparticles over halloysite clay mineral besides the pristine materials were used and evaluated to the photocatalytic decomposition of tebuconazole fungicide in water. The textural properties of the samples were analyzed by nitrogen (N_2) sorption and desorption porosimetry. The hysteresis loop appears to a high relative pressure region ($0.8 < P/P_o < 1.0$), which suggests that TiO_2 particles of all samples, form large pores. The BET specific surface area (SSA) for pristine halloysite and commercial TiO_2 powder (P25-TiO_2) is 47 and 50 m^2/g respectively. Surprisingly, the SSA of the composite halloysite/TiO_2 system is much higher ranging at 187–222 m^2/g depending on the quantity of TiO_2. We attribute the very high values of SSA to the hydrothermal treatment of the composite material which usually leads to the formation of highly porous TiO_2 at relatively low temperature and also to the good dispersion of the TiO_2 particles onto the halloysite nanotubes. The total pore volume (V_p) ranged from 0.25 to 0.35 cm^3/g for all samples. The BET SSA, the V_p, and the total porosity (φ) for all samples are presented in Table 1.

The equation for the calculation of the total porosity is given as follows:

$$\varphi = \frac{V_p}{\frac{1}{3.8} + V_p} \tag{4}$$

From the values obtained it can be seen that the less porous sample is the commercial P25-TiO_2, while the sample with the highest porosity is the composite halloysite 10%–TiO_2 90%.

Table 1
Structural characteristics of photocatalysts used

Sample	Basal spacing d (001)	Total pore volume (V_p) (cm^3/g)	S_{BET} (m^2/g)	ϕ (%)
P25-TiO_2	–	0.25	50	48.7
Halloysite	7.40	0.29	47	52.5
Halloysite 10%–TiO_2 90% (Hal 10– TiO_2 90)	7.29	0.35	222	57.1
Halloysite 30%–TiO_2 70% (Hal 30–TiO_2 70)	7.29	0.34	187	56.7
Halloysite 40%–TiO_2 60% (Hal 40–TiO_2 60)	7.29	0.35	188	57.1

XRD patterns were used to identify the crystal phase and the size of the as-synthesized nanocomposite TiO_2 besides the halloysite nanocomposite clay. Fig. 2 shows the results of XRD patterns of the three composite halloysite/TiO_2 samples. Nanocomposite's XRD patterns show only the presence of halloysite 7 Å and anatase, confirming the samples phase purity, while the intensities of basal reflections of halloysite 7 Å are significantly smaller than those of pure anatase, especially in the nanocomposite with the lowest amount (10%) of halloysite (Fig. 2). The XRD patterns of the prepared nanocomposites showed all the characteristic reflections of anatase (γ-TiO_2), which are marked in Fig. 2. For the samples, intense peaks at 2-theta angles of 25.3°, 37.5°, 48.01°, and 55.0° can be observed, which suggests that there is pure anatase crystal phase (Fig. 2).

The average size of the crystallites was determined using the Scherrer's semi-empirical equation (5) for the strongest Bragg peaks:

$$d = \frac{K\lambda}{\beta \cos\theta} \tag{5}$$

where λ is the wavelength of X-rays (0.154 nm), β is the full width at half-maximum (FWHM) in radian, and θ is the Bragg angle. Taking into account the FWHM of anatase (101) plane both samples exhibited approximately the same crystal size 14–16 nm.

The XRD patterns also indicated that the relatively increased temperature (180°C) of the hydrothermal treatment

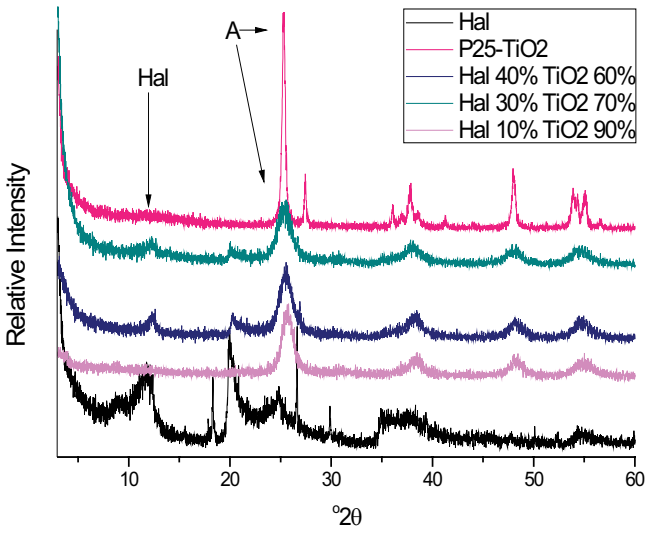

Fig. 2. XRD patterns of pristine halloysite, P25-TiO_2, and halloysite–TiO_2 nanocomposites at different ratios. (Hal: Halloysite, A: Anatase).

of the halloysite–TiO_2 nanocomposites did not modify the native halloysite 7 Å structure [24].

The morphology of halloysite and composite halloysite/TiO_2 samples was examined by FE-SEM microscopy (Fig. 3), where surface image of the samples showed the grain growth structure. Mostly, the grain boundaries are relatively regular

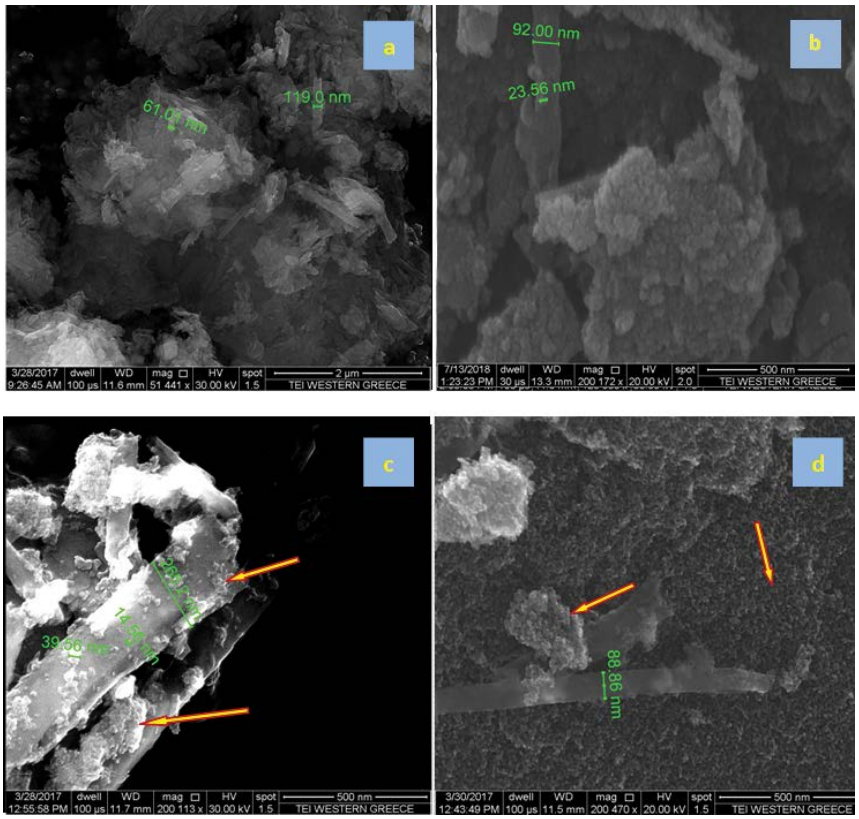

Fig. 3. SEM images: (a) Halloysite nanotubes morphology, (b) Hal 30–TiO_2 70 sample, (c) Hal 40–TiO_2 60 sample, and (d) Hal 10–TiO_2 90 sample. The arrows indicate the TiO_2 nanoparticles on the halloysite nanotubes.

and less aggregated, delineating a homogeneous composition with uniform porous allocation. SEM observations showed that TiO_2 in the crystal form of anatase was well fabricated on the halloysite nanotubes. SEM images of the nanocomposites showed that many uniform TiO_2 grains of less than 30 nm in size were deposited on the external surfaces of halloysite tubes (Figs. 3 (b)–(d)). The TiO_2 nanoparticles were found to be distributed very well on halloysite external surfaces but not homogeneously, which would be the ideal but rather impossible or at least unexpected. TiO_2 nanoparticles seem to partially cover the lumen of many halloysite tubes (Figs. 3 (b)–(d)). In the case of halloysite, an average width of 88–300 nm and average length of 1,000–1,200 nm was observed.

The dispersed TiO_2 nanoparticles in the size of 14–30 nm depending on the aggregation level were also monitored in Figs. 3 (b)–(d). The size of the TiO_2 nanoparticles as it was observed in SEM images is in good agreement with calculated average size from XRD data. Additionally, high-resolution TEM images clearly present the dense and homogeneous TiO_2 nanocrystals (Fig. 4) with average particle size of 3–10 nm, and lattice spacing of TiO_2 particles to be approximately 0.35 ± 0.02 nm (measured in higher magnification, not presented herein), indicating that it belonged to the (101) crystallographic plane of anatase type as was also found by XRD presented in Fig. 2.

In order to estimate the photodecomposition rate (r) of TEB fungicide, we employed the following equation:

$$r = \frac{\left(C_o - C\right)}{C_o} \tag{6}$$

where C_o is the initial concentration of the pollutant (TEB in our case) measured in solution and C is the final concentration after irradiation with UV light. Then we can calculate the degradation efficiency (e%) as follows:

$$e\% = \frac{\left(C_o - C\right)}{C_o} \times 100\% \tag{7}$$

As it was expected, the pristine halloysite sample did not perform any photocatalytic effect to the TEB fungicide. In addition, the photocatalytic efficiency of TiO_2 P25 is lower than the halloysite–TiO_2 nanocomposites. The highest photocatalytic efficiency, 47.4%, was achieved with the halloysite 10%–TiO_2 90% sample because of the higher photocatalyst

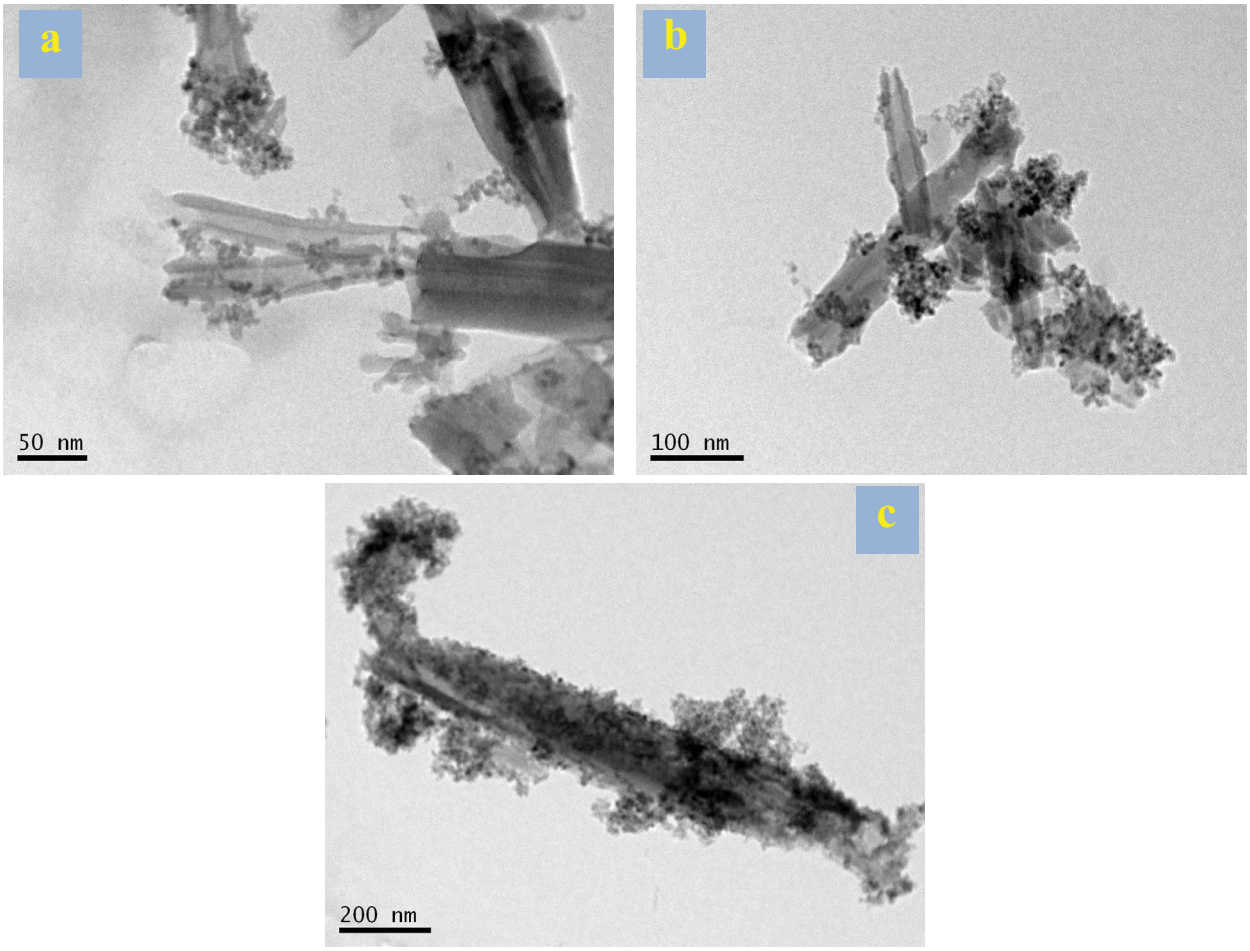

Fig. 4. TEM images presenting TiO_2 grains of about 3–10 nm on TiO_2-halloysite samples: (a) Hal 40–TiO_2 60, (b) Hal 30–TiO_2 70, and (c) Hal 10–TiO_2 90.

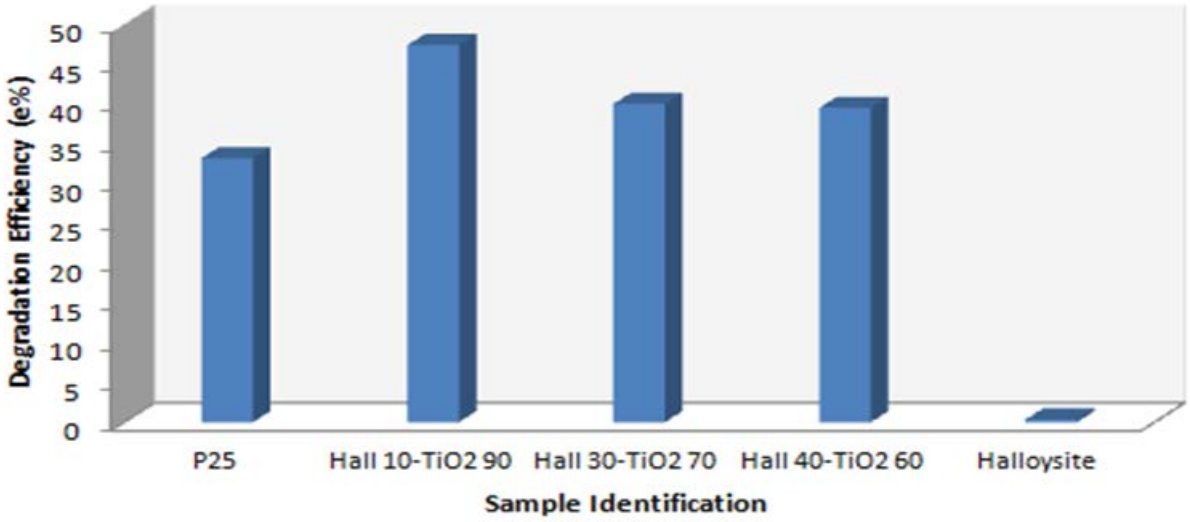

Fig. 5. Degradation efficiency of TEB.

proportion and the high SSA 222 m^2/g, among all the materials used. The halloysite 40%–TiO_2 60% and halloysite 30%–TiO_2 70% sample also shows better degradation efficiency compared with P25-TiO_2 but lower photocatalytic activity than the halloysite 10%–TiO_2 90% nanocomposite. This is probably due to the relatively lower amount of the photocatalyst (anatase) despite the relatively better dispersion of the TiO_2 photocatalyst on the halloysite nanotubes (Figs. 4(a)–(c) and 5).

The P25-TiO_2 decomposition efficiency reaches a maximum of 33.2% after 240 min of irradiation, while the halloysite 30%–TiO_2 70% and the halloysite 40%–TiO_2 60% nanocomposite shows 40.0% and 39.5%, respectively, degradation efficiency in the same period of time.

The concentration variation of TEB fungicide in aqueous solution with time under UV irradiation in the presence of photocatalysts was also monitored with TOC measurements appear in Fig. 6(a). All the data obtained after 1°h of fungicide's presence with catalyst in dark in order to reach absorption equilibrium. After 150 min of illumination no change was observed for the photodegradation of TEB for all samples studied. It should be noted that the halloysite 30%–TiO_2 70% and the halloysite 40%–TiO_2 60% nanocomposites show lower photocatalytic activity than halloysite 10%–TiO_2 90% despite the significantly lower amount of the anatase and very well dispersion on halloysite tubes. The halloysite substrate acts as an efficient absorbent of the organic contaminant accelerating the removal of TEB from solution by a better mass transfer of the pollutant to the TiO_2 photocatalyst surface. In addition, the halloysite clay mineral prevents the agglomeration of the TiO_2 nanoparticles. This phenomenon enhances TEB accessibility to the TiO_2 surface, resulting to

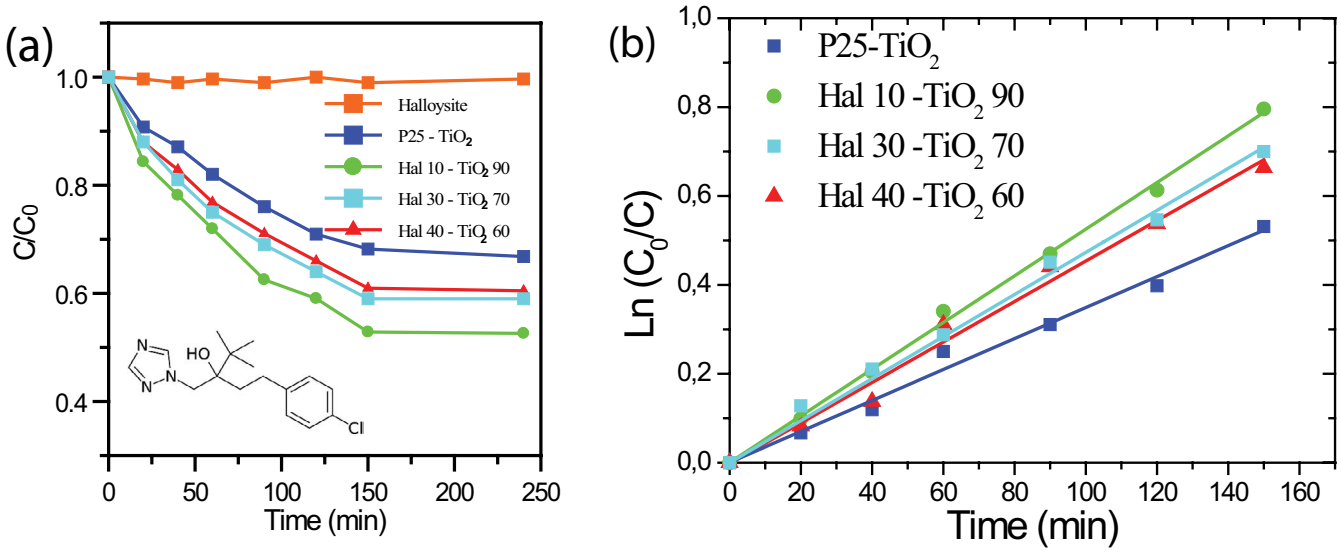

Fig. 6. (a) TEB decomposition with time of irradiation in the presence of various photocatalysts. Inset: The chemical formula of TEB. (b) $\ln(C_o/C)$ of TEB as a function of irradiation time.

a higher degree of irradiation exposure as well as a better photocatalytic performance of the catalyst.

For each case, the constant rate (k_{app}) was calculated by the slope of the lines in the graphs of $\ln(C_o/C)$ versus irradiation time (Fig. 6(b)). The maximum value was calculated for the halloysite 10%–TiO_2 90% sample (5.2×10^{-3} min^{-1}), without substantial reduction over repetitions. The constant rate for halloysite 30%–TiO_2 70% and halloysite 40%–TiO_2 60% sample was found to be a few lower (4.9×10^{-3} and 4.8×10^{-3} min^{-1}, respectively), while for P25-TiO_2 sample the constant rate was even lower (3.5×10^{-3} min^{-1}). It is obvious that the content of TiO_2 nanoparticles strongly influences the reaction rate of TEB decomposition.

For the reproducibility in the long term, the halloysite 10%–TiO_2 90% photocatalyst was tested three times for TEB degradation. Finally, it has been proved that the halloysite 10%–TiO_2 90% powder doesn't present any notable loss to its efficiency for TEB destruction. Specifically, diminish of the dissociation rate over repetition times doesn't exceed 5.4% for TEB fungicide.

4. Conclusions

In this study, the photocatalytic performance of new halloysite–TiO_2 nanocomposites was examined. We synthesized halloysite 10%–TiO_2 90%, halloysite 30%–TiO_2 70%, and halloysite 40%–TiO_2 60% nanomaterials. The characterization of the new composites showed that the anatase form of TiO_2 was apparent and well dispersed onto the halloysite nanotubes. The new materials have high SSAs of 187, 188, and 222 m^2/g for the halloysite 30%–TiO_2 70%, the halloysite 40%–TiO_2 60%, and the halloysite 10%–TiO_2 90%, respectively. The photocatalytic decomposition of TEB was performed under UV illumination for 240 min. The results indicated that the new halloysite–TiO_2 nanocomposites can be used as effective catalysts for the photodecomposition of TEB in water in comparison with P25-TiO_2. Indeed, the decomposition efficiency of P25-TiO_2, halloysite 40%–TiO_2 60%, halloysite 30%–TiO_2 70%, and halloysite 10%–TiO_2 90% was 33.2%, 39.5%, 40.0%, and 47.4%, respectively. In addition, the maximum 47.4% of tebuconazole content has been decomposed within first 150 min under UV irradiation, while no further photocatalytic activity was observed the last 90 min of UV exposure.

Acknowledgments

The authors would like to thank Applied Minerals Inc., New York, USA, for providing us the clay mineral halloysite.

References

[1] FAO/ECE, Legislation and Measures for the Solving of Environmental Problems Resulting from Agricultural Practices (With Particular Reference to Soil, Air and Water), Their Economic Consequences and Impact on Agrarian Structures and Farm Rationalization. United Nations Economic Commission for Europe (UNECE) and FAO, Agri/Agrarian Structures and Farm Rationalization, report No. 7, 1991.
[2] World Health Organization, Guidelines for Drinking-Water Quality, vol. 1, Recommendations, 2nd ed., WHO, Geneva, 1993.
[3] RIVM, The Environment in Europe: A Global Perspective, National Institute of Public Health and Environmental Protection (RIVM), Netherlands, 1992.
[4] S. Reichenberger, M. Bach, A. Skitschak, H.G. Frede, Mitigation strategies to reduce pesticide inputs into ground- and surface water and their effectiveness: a review, Sci. Total Environ., 384 (2007) 1–35.
[5] I.K. Konstantinou, T.A. Albanis, Photocatalytic transformation of pesticides in aqueous titanium dioxide suspensions using artificial and solar light: intermediates and degradation pathways, Appl. Catal., B, 42 (2003) 319–335.
[6] N. Vela, M. Calín, M.J. Yáñez-Gascón, I. Garrido, G. Pérez-Lucas, J. Fenoll, S. Navarro, Photocatalytic oxidation of six pesticides listed as endocrine disruptor chemicals from wastewater using two different TiO_2 samples at pilot plant scale under sunlight irradiation, J. Photochem. Photobiol., A, 353 (2018) 271–278.
[7] S. Malato, P. Fernández-Ibáñez, M.I. Maldonado, J. Blanco, W. Gernjak, Decontamination and disinfection of water by solar photocatalysis: recent overview and trends, Catal. Today, 147 (2009) 1–59.
[8] S. Ahmed, M.G. Rasul, R. Brown, M.A. Hashib, Influence of parameters on the heterogeneous photocatalytic degradation of pesticides and phenolic contaminants in wastewater: a short review, J. Environ. Manage., 92 (2011) 311–330.
[9] I. Fechete, Y. Wang, C. Védrine, The past, present and future of heterogeneous catalysis, Catal. Today, 189 (2012) 2–27.
[10] R. Dewil, D. Mantzavinos, I. Poulios, M.A. Rodrigo, New perspectives for advanced oxidation processes, J. Environ Manage., 195 (2017) 93–99.
[11] M.M. Mahlambi, C.J. Ngila, B.B. Mamba, Recent developments in environmental photocatalytic degradation of organic pollutants: the case of titanium dioxide nanoparticles – a review, J. Nanomat., 2015 (2015) 1–29.
[12] A.O. Ibhadon, P. Fitzpatrick, Heterogeneous photocatalysis: recent advances and applications, Catalysts, 3 (2013) 189–218.
[13] R. Fagan, D.E. McCormack, D.D. Dionysiou, S.C. Pillai, A review of solar and visible light active TiO_2 photocatalysis for treating bacteria, cyanotoxins and contaminants of emerging concern, Mater. Sci. Semicond. Process., 42 (2016) 2–14.
[14] Y. Nosaka, A. Nosaka, Understanding hydroxyl radical (•OH) generation processes in photocatalysis, ACS Energy Lett., 1 (2016) 356–359.
[15] G.V. Buxton, C.L. Greenstock, W.P. Helman, A.B. Ross, Critical review of rate constants for reactions of hydrated electrons, hydrogen atoms and hydroxyl radicals (•OH/•O^-) in aqueous solution, J. Phys. Chem., 17 (1988) 513–886.
[16] G.P. Anipsitakis, D.D. Dionysiou, Radical Generation by the interaction of transition metals with common oxidants, Environ. Sci. Technol., 38 (2004) 3705–3712.
[17] P. Neta, R.E. Huie, A.B. Ross, Rate constants for reactions of inorganic radicals in aqueous solution, J. Phys. Chem. Ref. Data, 17 (1988) 1027–1284.
[18] M.R. Hoffmann, S.T. Martin, W. Choi, D.W. Bahnemann, Environmental applications of semiconductor photocatalysis, Chem. Rev., 95 (1995) 69–96.
[19] M.I. Litter, Heterogeneous photocatalysis: transition metal ions in photocatalytic systems, Appl. Catal., B, 23 (1999) 89–114.
[20] N. Stamatis, M. Antonopoulou, I. Konstantinou, Photocatalytic degradation kinetics and mechanisms of fungicide tebuconazole in aqueous TiO_2 suspensions, Catal. Today, 252 (2015) 93–99.
[21] P. Calza, S. Baudino, R. Aigotti, C. Baiocchi, P. Branca, E. Pelizzetti, High-performance liquid chromatographic/tandem mass spectrometric identification of the phototransformation products of tebuconazole on titanium dioxide, J. Mass Spectrom., 37 (2002) 566–576.
[22] T. De Hermann Prestes, D. De Oliveira Gibbon, M.A. Lansarin, C.C. Moro, Tebuconazole photocatalytic degradation kinetics, Quim. Nova, 33 (2010) 798–801.
[23] D. Papoulis, S. Komarneni, D. Panagiotaras, E. Stathatos, K.C. Christoforidis, M. Fernández-García, H. Li, S. Yin, T. Sato, H. Katsuki, Three-phase nanocomposites of two nanoclays and TiO_2: Synthesis, characterization and photacatalytic activities, Appl. Catal., B, 147 (2014) 526–533.

[24] D. Papoulis, S. Komarneni, D. Panagiotaras, E. Stathatos, D. Toli, K.C. Christoforidis, M. Fernández-García, H. Li, S. Yin, T. Sato, H. Katsuki, Halloysite–TiO_2 nanocomposites: synthesis, characterization and photocatalytic activity, Appl. Catal., B, 132–133 (2013) 416–422.
[24] D. Papoulis, S. Komarneni, D. Panagiotaras, A. Nikolopoulou, H. Li, S. Yin, T. Sato, H. Katsuki, Palygorskite–TiO_2 nanocomposites: Part 1. Synthesis and characterization, Appl. Clay Sci., 83–84 (2013) 191–197.
[26] D. Papoulis, S. Komarneni, D. Panagiotaras, A. Nikolopoulou, K.C. Christoforidis, M. Fernández-García, H. Li, S. Yin, T. Sato, Palygorskite–TiO_2 nanocomposites: Part 2. Photocatalytic activities in decomposing air and organic pollutants, Appl. Clay Sci., 83–84 (2013) 198–202.
[27] G. Shankaraiah, S. Poodari, D. Bhagawan, Vurimindi Himabindu, S. Vidyavathi, Degradation of antibiotic norfloxacin in aqueous solution using advanced oxidation processes (AOPs) – a comparative study, Desal. Wat. Treat., 57 (2016) 27804–27815.
[28] L. Sun, C. Sun, X. Sun, Solar photocatalytic decolorization of azo dyes in water and textile wastewater on N-(Cr^{3+}, Fe^{3+}) doped-TiO_2 nanoparticle films: optimization of some operational parameters, Desal. Wat. Treat., 56 (2015) 346–355.
[29] A.D. Eaton, Standard Methods for the Examination of Water and Wastewater, 21st American Public Health Association, American Water Works Association, Water Environment Federation, APHA-AWWA-WEF, Washington, DC, 2005.
[30] V. Bekiari, P. Avramidis, Data quality in water analysis: validation of combustion-infrared and combustion-chemiluminescence methods for the simultaneous determination of Total Organic Carbon (TOC) and Total Nitrogen (TN), Int. J. Environ. Anal. Chem., 94 (2014) 65–76.